Polystyrene Nanocomposite Materials: Preparation, Morphology, and Mechanical, Electrical, and Thermal Properties

Chen-Chi M. Ma, Yi-Jie Chen, Hsu-Chiang Kuan

Department of Chemical Engineering, National Tsing-Hua University, Hsin-Chu, Taiwan 30043, Republic of China

Received 7 April 2004; accepted 10 September 2004
DOI 10.1002/app.22121
Published online in Wiley InterScience (www.interscience.wiley.com).

ABSTRACT: In this study, we prepared polystyrene (PS) resin nanocomposites with antistatic properties by melt-blending PS with nanoscale zinc oxide (ZnO). The effects of nanoscale ZnO on the electrical and physical characteristics of the PS nanocomposites were investigated. Two kinds of nanoscale powders, spherical zinc oxide (s-ZnO) and zinc oxide whisker (w-ZnO), were selected. The coupling agents vinyltriethoxysilane (VTES) and phenyltriethoxysilane (PTES) were used to improve the compatibility between the nanopowders and PS resin. The addition of s-ZnO and w-ZnO improved the antistatic characteristics of the materials. The surface resistivities of the s-ZnO and w-ZnO nanocomposites were significantly reduced by modification with VTES and PTES. The addition of ZnO nanopowder increased the flexural modulus and reduced the flexural strength. The silane coupling agents improved the flexural properties of the nanocomposites. The glass-transition temperatures and thermal degradation temperatures of the ZnO/PS nanocomposites increased with ZnO content. Treatment with silane increased the glass-transition temperatures and thermal degradation temperatures of the composites. J Appl Polym Sci 98: 2266–2273, 2005

Key words: polystyrene; nanoparticles; mechanical properties

INTRODUCTION

According to the properties of antistatic materials, one can divide prepare these materials by one of the following three methods:

1. Antistatic agents, such as nonionic surfactants or hydrophilic polymers, can be applied to the surface of products or blended into raw materials to form antistatic materials.[1–3]
2. The polymer matrix can be blended with conductive additives, such as carbon black,[4–6] metal powder,[7,8] or conductive fibers,[9,10] to form an antistatic polymer.
3. The molecular structure of the material that is originally conductive, such as a conducting polymer, can be used to prepare antistatic materials.[11–14]

Antistatic agents can be used as lubricants, which also offer conductive channels. Antistatic agents used as lubricants can lower the coefficient of friction of plastics and thus decrease the gathering of static charges around the surface.[15] This function, however, cannot disperse the static charges. The second function, instead, can offer conductive channels, which help to disperse the charges. It can also further release the charges. The main function of the antistatic agent is to offer conductive channels; a continuous water layer is usually formed due to the attachment of steam to the surface of the antistatic agents.[16] From previous research, it is known that proper absorptivity is a necessary property of antistatic agents. The conductivity of the water layer increases when the number of ions increases. As a result, the higher the ionic properties of the antistatic agents are, the better the antistatic properties of the composite materials will be.[17]

Because of its excellent properties and its lower price, carbon black, in the past decades, has been blended into polymer materials to provide conductivity to the materials.[4–6] Although carbon black can serve as a good conductive additive, it darkens the surface of plastic products, a fatal defect that makes coloring even more difficult.

Many studies have indicated that polymer composites prepared as a mixture of a conjugated conducting phase and a classical nonconducting phase show quite a good electrical conductivity at a relatively low content of the conducting phase.[11,12]

Furthermore, some studies have used the compositions of coating solutions including conductive metal

Correspondence to: C.-C. M. Ma (ccma@che.nthu.edu.tw).
Contract grant sponsor: National Science Council, Taiwan, Republic of China; contract grant number: NSC 91-2622-E-007-008.

oxide semiconductors, such as tin dioxide, indium(III) oxide, and zinc oxide (ZnO), dispersed in a binder, which may be either a nonconductive polymer or a polyelectrolyte. The coating layer gave excellent antistatic properties even at low humidities.[18]

In this study, we prepared antistatic polystyrene (PS) nanocomposite materials by incorporating nanoscale ZnO's. Two kinds of ZnO were used in this study, namely, spherical zinc oxide (s-ZnO) and zinc oxide whisker (w-ZnO). Two kinds of silane coupling agents, namely, vinyltriethoxysilane (VTES) and phenyltriethoxysilane (PTES), were used to improve the compatibility of inorganic ZnO and PS resin. They provided chemical (C—C bonding) and physical (π–π interaction) forces, respectively. The electrical, mechanical, and thermal properties and the morphologies of the nanocomposite materials are discussed in this article.

EXPERIMENTAL

Materials

General-purpose PS pellets with a weight-average molecular weight of 150,000 g/mol were received from the Chi-Mei Co. (Taiwan). The two kinds of silane coupling agents, VTES (CSH1S03Si) and PTES (C12H2003Si), were purchased from Lancaster Synthesis, Ltd. (Newgate, England) and Acros Co. (Janssens Pharmaceuticalaan 3A 2440, Geel, Belgium), respectively. Two kinds of nanoscale powders, s-ZnO and w-ZnO, were used. s-ZnO, with a particle size of about 31 nm and a specific surface area of about 11.1 m^2/g, was purchased from Nanophase Technologies Corp. (Romeoville, IL). w-ZnO, with a particle size of about 30 nm, a specific surface area of about 40–60 m^2/g, and an aspect ratio of about 5, was purchased from Nanjing High Technology Nano Co., Ltd. (Nanjing, China).

Modifying the surfaces with coupling agents

Nanoscale ZnO powders were dried for 24 h and then put into the reactor. VTES (CSH1S03Si) and PTES (C12H2003Si) were used as the coupling agents and were mixed with nanoscale ZnO powder. The weight ratio of the coupling agent to the nanoscale ZnO powder was 20 : 1. Tetrahydrofuran was used as a solvent, and a small amount of acetic acid potassium was used as a catalyst. The mixture was stirred at 60°C for 24 h. After the reaction was complete, we separated the mixture by centrifuging three times and then drying it in a vacuum oven.

Preparation of the ZnO/PS nanocomposites

The ZnO/PS nanocomposites were obtained by the mixture of the PS pellets with 0, 5, 10, 20, and 30 wt % ZnO filler with a Hakke mixer (Rheomix 600p, Thermo Electron Co., Hamburg, Germany) at 160°C for 5 min. With this process, the mixture was compressed into plaques for 15 min at 160°C and 10 MPa.

Property measurement characterization

Fourier transform infrared spectroscopy (FTIR)

FTIR spectra of the samples were recorded between 4000 and 400 cm^{-1} on a Nicolet Avatar 320 FTIR spectrometer (Nicolet Instrument Co., Madison, WI). We prepared the thin films by mixing the finely ground solid sample with powdered potassium bromide and pressing the mixture under a high pressure at 8000–10,000 kg/cm^2. A minimum of 32 scans was signal-averaged with a resolution of 2 cm^{-1} in the 4000–400-cm^{-1} range.

Scanning electron microscopy (SEM)

The morphologies of the fractured surfaces of the nanocomposites were examined by SEM (JEOL JSM 5300, Peabody, MA) to study the dispersion and size of the nanoscale ZnO powder in the polymer.

Flexural strength and flexural modulus test

The flexural strength and flexural modulus were measured according to ASTM D 790 with a test specimen bar 100 mm long, 13 mm wide, and about 3 mm thick. The supporting span was 60 mm, and the crosshead rate was 5 mm/min.

Surface resistivity test

The surface resistance of the composite was tested on a super-high-resistance meter (Megohmeter SME-8311, Dkk-Toa Co., Tokyo) according to ASTM D 257 with a test thin film 40 mm long and 40 mm wide. The test was conducted with a voltage of 1000 V, a charge of 30 s, a temperature of 25°C, and a relative humidity of 50%.

Differential scanning calorimetry (DSC)

DSC analyses of the samples were carried out under a N_2 atmosphere with a TA Instruments DSC 10 (TA Instruments, New Castle, DE). Samples were first placed in a vacuum oven at 100°C for 24 h before they were sealed in an aluminum sample cell and then held at 100°C for 10 min. They were then quickly put into liquid nitrogen until a temperature of −100°C was reached to obtain amorphous samples. These amorphous samples were then heated again to 100°C at a heating rate of 10 K/min.

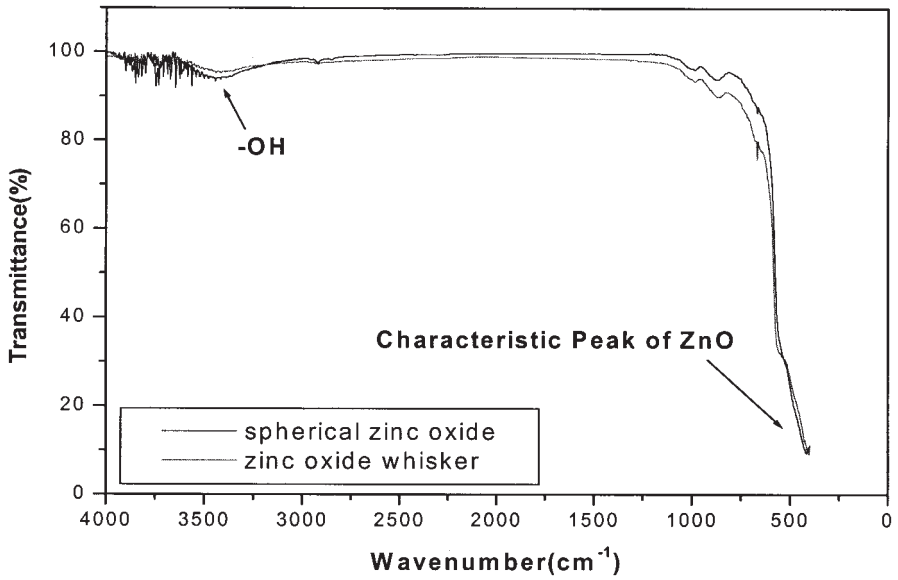

Figure 1 FTIR spectra of different types of ZnO nanoparticles.

Thermogravimetric analysis (TGA)

The thermal degradation properties of the nanocomposites were measured by TGA (DuPont-951, New Castle, DE) from room temperature to 600°C at a heating rate of 10 K/min under a N_2 atmosphere. The weight loss-to-temperature curves were recorded with 6–10-mg samples.

RESULTS AND DISCUSSION

Analysis of the functional groups on the surfaces of the ZnO's

Figure 1 presents the FTIR spectra of nanoscale s-ZnO and w-ZnO. The spectra exhibited a weak absorption peak at 3400 cm^{-1}. The absorption peak ranged from 3000 to 3600 cm^{-1}, a range that corresponded to the hydroxy group, —OH, which confirmed that the surfaces of the two selected nanoscale ZnO powders contained —OH groups. Furthermore, the strong absorption that appeared at about 400 cm^{-1} was a diagnostic absorption peak of ZnO.

Surface resistivities of the ZnO/PS nanocomposites

Figure 2 depicts the surface resistivities of two ZnO/PS nanocomposite materials. The surface resistivities fell as ZnO increased. The addition of 30 wt % s-ZnO and w-ZnO reduced the surface resistivities of materials from $1.0 = 10^{16}$ to $8.98 = 10^{12}$ and to 9.57×10^{10} Ω/cm^2, respectively. The amount of ZnO in the PS resin could be gradually increased to form a conductive network in the materials.

The surface resistivity of the w-ZnO/PS nanocomposite materials was two orders less than that of the s-ZnO/PS nanocomposite materials, perhaps for the following reasons:

1. Conductive network: Because the aspect ratio of w-ZnO (5) was higher than that of s-ZnO (1), w-ZnO was more efficient than s-ZnO in the formation of a conductive network, and hence, it produced a lower surface resistivity.
2. The charge-concentrating effect at the pinpoint:[19] According to the results of Zhou et al.,[19] the intensity of the surface electrons of whisker (whose aspect ratio was 10) is 400 times higher than that of general spherical particles. The conspicuous charge-concentrating effect may have caused the polymer matrix between the tips of the whiskers to be broken down; the effect would therefore result in conductivity.

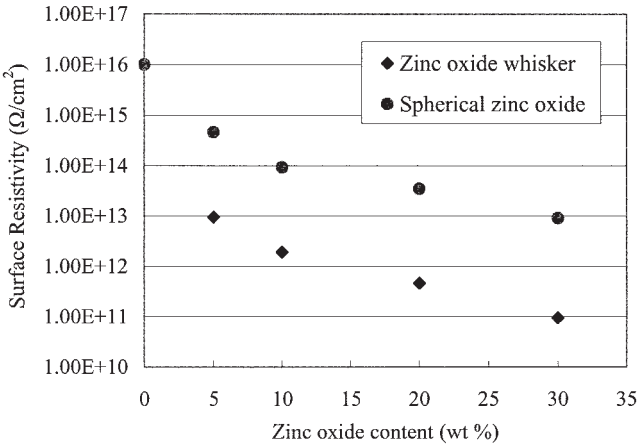

Figure 2 Surface resistivities of ZnO/PS nanocomposites with different types of ZnO nanoparticles.

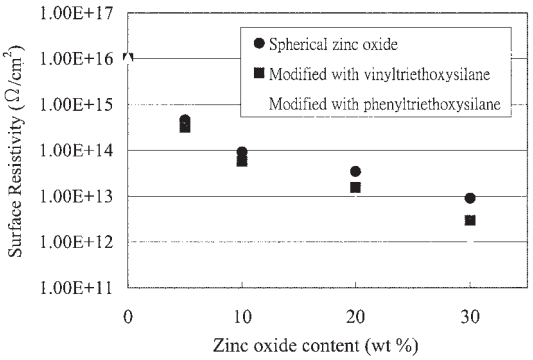

Figure 3 Surface resistivities of s-ZnO/PS nanocomposites with different modifiers.

3. Tunnel effect:[19] The *tunnel effect* refers to the phenomenon of current leakage within the materials. The following equation regarding the charge carrier and penetrating probability explains this phenomenon:

$$p = \exp\left[-\frac{2L}{\hbar} \sqrt{2m(V_0 - E)} \right] \quad (1)$$

where p is the penetrating probability; L is the distance between the charge carriers; m is the mass of the charge carrier; $\hbar = h/2\pi$, where h is Planck's constant and is equal to 6.63×10^{-34} J s; and $(V_0 - E) = 1.6 \times 10^{-19}$ J in the electronic system. V_0 is the level energy of ground state and E is the level energy at infinite level.

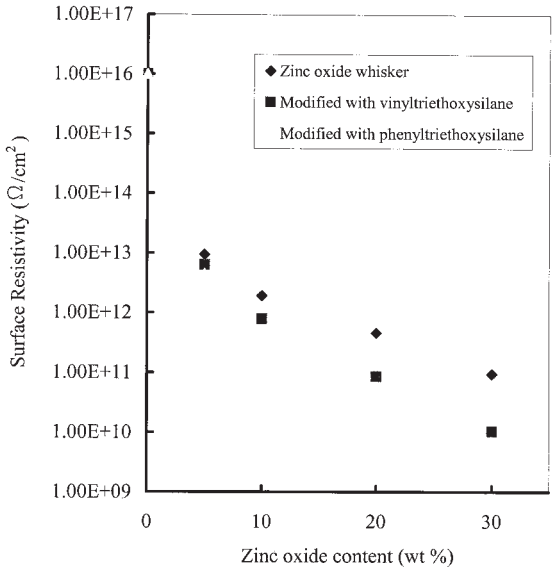

Figure 4 Surface resistivities of w-ZnO/PS nanocomposites with different modifiers.

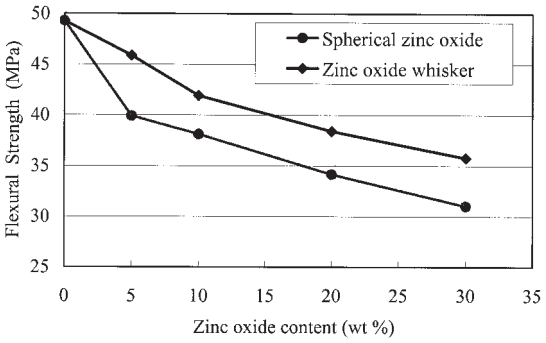

Figure 5 Flexural strengths of ZnO/PS nanocomposites with different types of ZnO nanoparticles.

Equation (1) reveals that the penetrating probability is inversely proportional to the distance between charge carriers. Restated, the addition of only a small quantity of whisker is not likely to cause the tunnel effect. The tunnel effect clearly affects the conductivity of the material when more than a certain amount is added.

Both Figures 3 and 4 indicate that the PS nanocomposites with modified s-ZnO or w-ZnO had lower surface resistivities than those to which no modified ZnO was added. The addition of 30 wt % s-ZnO and w-ZnO modified with VTES decreased the surface resistivities of the materials from 1.0×10^{16} to 2.95×10^{12} and 1.05×10^{10} Ω/cm^2, respectively. The surface resistivities of both materials with 30 wt % s-ZnO and w-ZnO modified with PTES fell to 9.98×10^{11} and 5.27×10^{9} Ω/cm^2, respectively. The modified ZnO could be easily dispersed in the resin, so the compatibility between PTES and the PS resin was also considerably improved. The modified ZnO was more effective than VTES in reducing the surface resistivity of the materials.

Flexural properties of the ZnO/PS nanocomposites

Figures 5–10 show plots of the flexural strengths and flexural moduli of various ZnO/PS nanocomposite

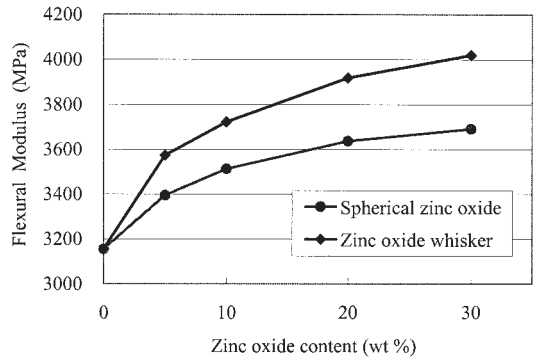

Figure 6 Flexural moduli of ZnO/PS nanocomposites with different types of ZnO nanoparticles.

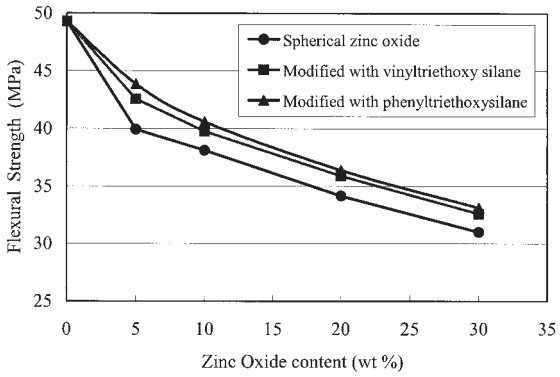

Figure 7 Flexural strengths of s-ZnO/PS nanocomposites with different modifiers.

materials. The flexural moduli of the materials increased and the flexural strengths of the materials declined as the ZnO content increased. The flexural moduli of the materials with 30 wt % s-ZnO and w-ZnO were 17.1 and 27.6%, higher, respectively, than that of the pure PS resin. The flexural strengths of the materials were 37.1 and 27.4% lower than that of the pure PS resin. The dispersion was poor when the rigid nano-ZnO was added to the highly viscous PS resin. Additionally, the high surface energy of the nanoparticles may have caused the nanoparticles to aggregate, and the stress may have concentrated within the aggregation. Hence, the strengths of the nanomaterials were reduced, and the modulus was increased.

Figure 5 and 6 reveal that the PS nanocomposites with 5, 10, 20, and 30 wt % w-ZnO had higher flexural strengths and flexural moduli than those of the materials with the same proportions of s-ZnO. w-ZnO has a unique structure, so a whisker was easily inserted into PS resin, increasing the contact area between the w-ZnO and the PS resin. Moreover, from the perspective of the reinforcement of the composite, w-ZnO increased the flexural strength and flexural modulus because it had a higher aspect ratio.

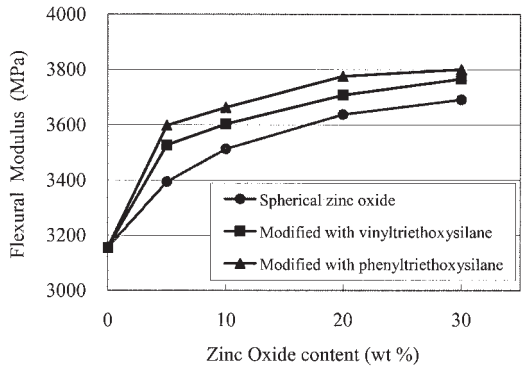

Figure 8 Flexural moduli of s-ZnO/PS nanocomposites with different modifiers.

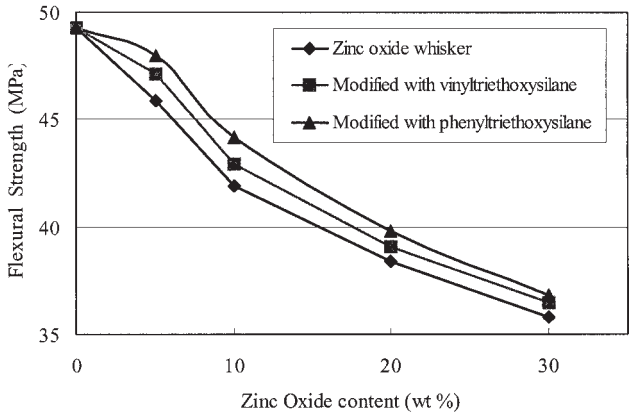

Figure 9 Flexural strengths of w-ZnO/PS nanocomposite with different modifiers.

Figure 7 to 10 demonstrate that the addition of only a small amount of the two modifiers increased the flexural strengths and flexural moduli of the nanomaterials. However, the influence of the modifiers on the flexural strength and the flexural modulus of the materials may have fallen as the quantity of the modifier increased. The flexural moduli of the materials with 30 wt % s-ZnO and w-ZnO modified with VTES were 19.7 and 30.5% higher, respectively, than those of the pure PS resin. The flexural strengths of the materials were 33.9 and 26.0% lower, respectively, than that of the pure PS resin. The flexural moduli of the materials modified with PTES were 20.6 and 32.7% higher, respectively, than those of the pure PS resin. The flexural strengths of the materials were 32.9 and 25.4% lower, respectively, than that of the pure PS resin. These figures show that PTES affected the flexural strengths and flexural moduli of the materials more strongly than VTES did. The chemical structure of PTES made it more compatible with the PS resin. Finally, the modified nanoparticles exhibited strong molecular interactions with the PS polymer chains.

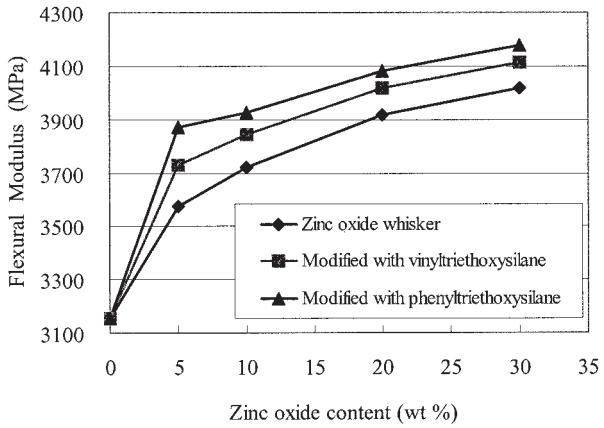

Figure 10 Flexural moduli of w-ZnO/PS nanocomposites with different contents and types of modifiers.

Morphologies of the ZnO/PS nanocomposites

Figures 11 and 12 present the morphologies of the ZnO/PS nanocomposites. The analyses of the morphological characteristics revealed that the particle size of unmodified s-ZnO (s-ZnO in Fig. 11) and unmodified w-ZnO (w-ZnO in Fig. 12) were 200–300 nm when the filler content reached 10 wt %. If a silane coupling agent was added, the particle size of ZnO (s-ZnO and w-ZnO) was smaller than 100 nm. When the ZnO content was 30 wt %, the particle size of the modified ZnO (s-ZnO and w-ZnO) was around 200–

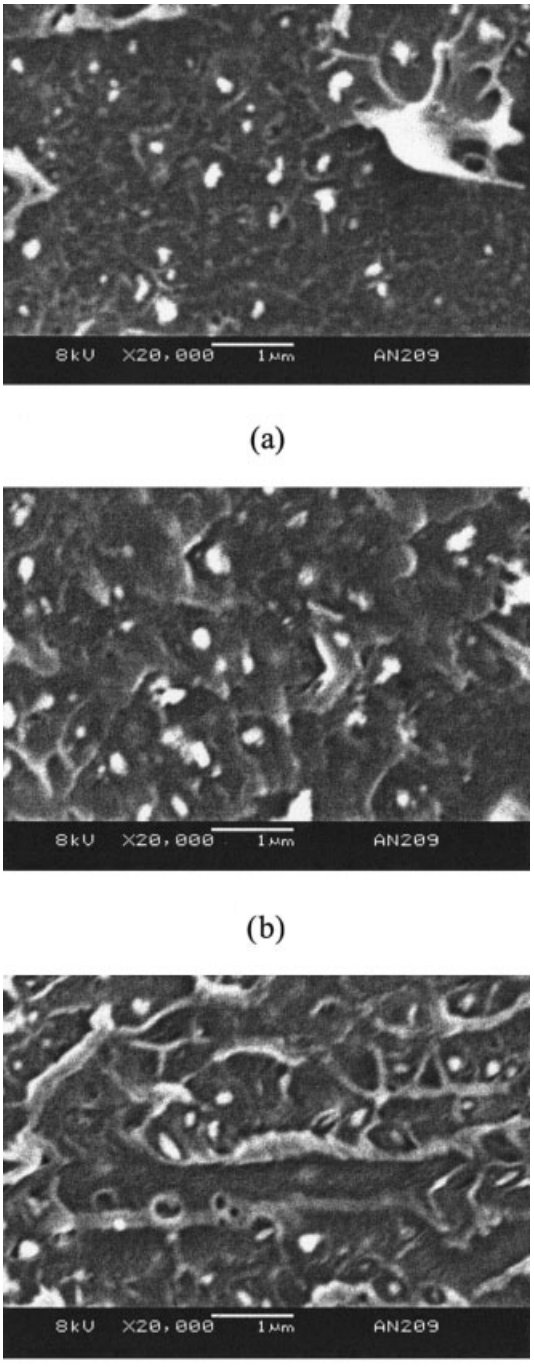

Figure 11 SEM microphotographs of s-ZnO/PS nanocomposites (20,000×) with various contents and types of coupling agents: (a) 10 wt %, (b) 30 wt % VTES-modified, and (c) 30 wt % PTES-modified s-ZnO/PS nanocomposites.

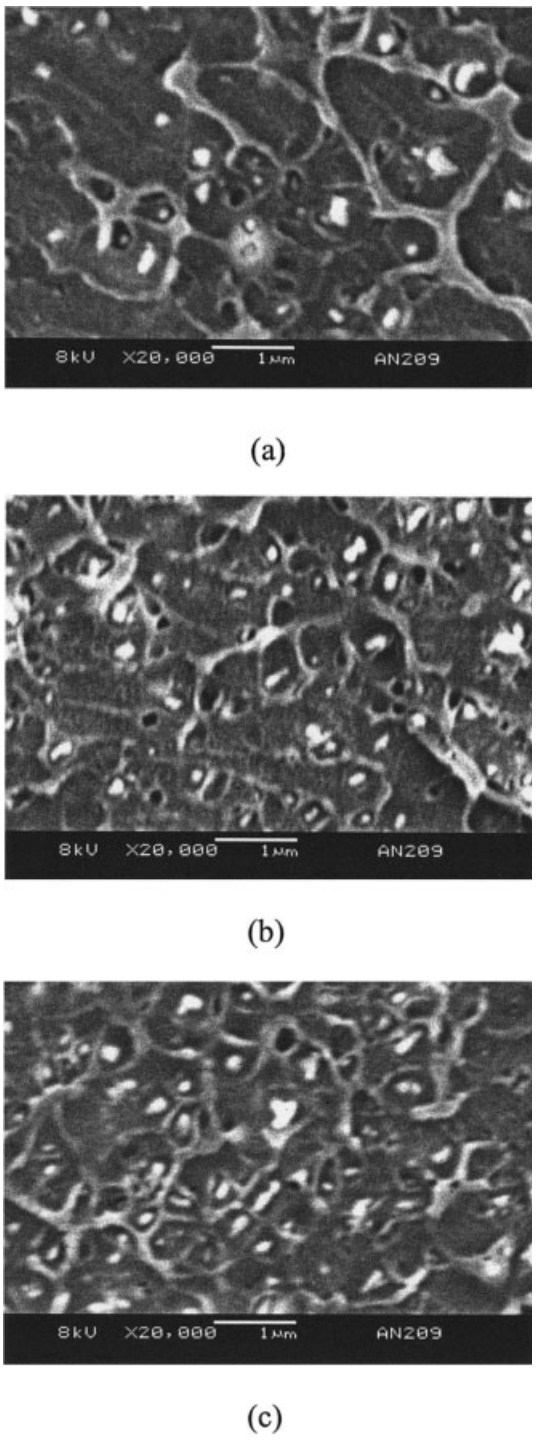

Figure 12 SEM microphotographs of w-ZnO/PS nanocomposites (20,000×) with various contents and types of coupling agents: (a) 10 wt %, (b) 30 wt % VTES-modified, and (c) 30 wt % PTES-modified w-ZnO/PS nanocomposites.

TABLE I
T_g Values of ZnO/PS Nanocomposites with Various s-ZnO and w-ZnO Contents

s-ZnO content (wt %)	T_g (°C)	w-ZnO content (wt %)	T_g (°C)
0	87.6	0	87.6
5	92.0	5	93.0
10	92.5	10	93.6
20	93.0	20	94.1
30	93.6	30	94.7

TABLE III
T_g Values of ZnO/PS Nanocomposites with VTES- and PTES-modified w-ZnO

VTES-modified w-ZnO content (wt %)	T_g (°C)	PTES-modified w-ZnO content (wt %)	T_g (°C)
0	87.6	0	87.6
5	93.4	5	93.9
10	94.0	10	94.6
20	94.7	20	96.1
30	95.7	30	97.3

300 nm. The results indicate that silane coupling agents were effective dispersion agents for the ZnO.

Glass-transition temperatures (T_g's) of the ZnO/PS nanocomposites

Tables I–III summarize the DSC analysis of the ZnO/PS nanocomposites. T_g of the ZnO/PS nanocomposites increased with ZnO content because ZnO restricted the segmental motion of the PS molecules and reduced the free volume of polymer chain folding. For instance, T_g of ZnO/PS nanocomposite increased from 87.6 to 93.6°C (s-ZnO) and 94.7°C (w-ZnO). W-ZnO had a larger aspect ratio than s-ZnO, so its restriction of molecular chain mobility exceeded that of s-ZnO. Nanocomposites treated with VTES and PTES exhibited higher T_g's. T_g's of 30 wt % s-ZnO with VTES and PTES treatment were 94.8 and 95.6°C, respectively. T_g's of 30 wt % w-ZnO with VTES and PTES treatment were 95.7 and 97.3°C, respectively. ZnO was effectively dispersed in the PS matrix treated with silane, so T_g of the nanocomposite increased as the silane was added.

Thermal stability of the ZnO/PS nanocomposites

Tables IV–VI demonstrate the thermal decomposition behavior of the ZnO/PS nanocomposites. The results indicate that the addition of ZnO may have increased the thermal degradation temperature. For example, the thermal degradation temperature associated with a 10 wt % weight loss (T_{d10}) of the ZnO/PS nanocomposite increased from 326 to 362°C (s-ZnO) and 374°C (w-ZnO). ZnO is an inorganic material that exhibits heat resistance, so the presence of ZnO may have retarded or delayed the onset of the thermal degradation of the PS. W-ZnO had a higher specific surface area (for the same amount added) than that of s-ZnO, so the former had a greater contact surface with PS, which increased the thermal stability of the nanocomposite. The nanocomposites treated with VTES and PTES exhibited higher thermal degradation temperatures. T_{d10}'s of 30 wt % s-ZnO treated with VTES and PTES were 372 and 374°C, respectively. T_{d10}'s of 30 wt % w-ZnO treated with VTES and PTES were 384 and 392°C, respectively. ZnO was effectively dispersed in the PS matrix treated with silane, so the thermal degradation temperature of the nanocomposite increased as the silane was added.

CONCLUSIONS

1. The surface resistivity study revealed that the addition of s-ZnO and w-ZnO improved the antistatic characteristics of the materials. The addition of 30 wt % s-ZnO and w-ZnO reduced the surface resistivities of the materials from 1.0 $\times$ 10^{16} to 8.98 $\times$ 10^{12} and 9.57 $\times$ 10^{10} Ω/cm^2, respectively. The addition of the same quantities of s-ZnO and w-ZnO reduced the surface resistivities of the materials modified with VTES to 2.95 $\times$ 10^{12} and 1.05 $\times$ 10^{10} Ω/cm^2, respectively. The surface resistivities of both materials modified with PTES were lower, at 9.98 $\times$ 10^{11} and 5.27 $\times$ $l0^9$ Ω/cm^2, respectively.

TABLE II
T_g Values of ZnO/PS Nanocomposites with VTES- and PTES-Modified s-ZnO

VTES-modified s-ZnO content (wt %)	T_g (°C)	PTES-modified s-ZnO content (wt %)	T_g (°C)
0	87.6	0	87.6
5	93.1	5	93.3
10	93.5	10	93.9
20	94.2	20	94.7
30	94.8	30	95.6

TABLE IV
T_{d10} Values of s-ZnO/PS and w-ZnO/PS Nanocomposites with Various ZnO Contents

s-ZnO content (wt %)	T_{d10} (°C)	w-ZnO content (wt %)	T_{d10} (°C)
0	326	0	326
5	335	5	338
10	345	10	353
20	356	20	361
30	362	30	374

2. The flexural moduli of 30 wt % s-ZnO and w-ZnO nanocomposite were 17.1 and 27.6% higher, respectively, than those of pure PS resin,. The flexural strengths of the 30 wt % s-ZnO and w-ZnO nanocomposites were 37.1 and 27.4% lower, respectively. The flexural moduli of the 30 wt % s-ZnO and w-ZnO nanocomposites modified with VTES were 19.7 and 30.5% higher, respectively. The flexural strengths of the 30 wt % s-ZnO and w-ZnO nanocomposites were 33.9 and 26.0% lower, respectively. The flexural moduli of the 30 wt % s-ZnO and w-ZnO nanocomposites modified with PTES were 20.6 and 32.7% higher, respectively. The flexural strengths of 30 wt % s-ZnO and w-ZnO nanocomposite were 32.9 and 25.4% lower, respectively.
3. The morphologies of the ZnO/PS nanocomposites showed that the particle sizes were 200–300 nm when the filler content exceeded 10 wt % in the unmodified case. The addition of a silane coupling agent reduced the particle size of the ZnO powder until the ZnO content of the nanocomposite exceeded 20 wt %.
4. T_g's of the ZnO/PS nanocomposites increased with ZnO content. The composites treated with silane exhibited higher T_g's than the composites not so treated. The thermal degradation temperature of the ZnO/PS nanocomposites increased with ZnO content. Silane treatment increased the thermal degradation temperatures of the composites.

TABLE V
T_{d10} Values of ZnO/PS Nanocomposites with VTES- and PTES-modified s-ZnO

VTES-modified s-ZnO content (wt %)	T_{d10} (°C)	PTES-modified s-ZnO content (wt %)	T_{d10} (°C)
0	326	0	326
5	343	5	352
10	353	10	362
20	361	20	368
30	372	30	374

TABLE VI
T_{d10} Values of ZnO/PS Nanocomposites with VTES- and PTES-modified w-ZnO

VTES-modified w-ZnO content (wt %)	T_{d10} (°C)	PTES-modified w-ZnO content (wt %)	T_{d10} (°C)
0	326	0	326
5	365	5	370
10	371	10	375
20	377	20	382
30	384	30	392

References

1. Kale, V.; Moukwa, M. J Electrostatics 1996, 38, 239.
2. Dacre, B.; Hetherington, J. I. J Electrostatics 1998, 45, 53.
3. Dudler, V.; Grob, M. C. Polym Degrad Stab 2000, 68, 373.
4. Ghosh, P.; Chakrabarti, A. Eur Polym J 2000, 36, 1043.
5. Pantea, D.; Darmstadt, H.; Kaliaguine, S.; Summchen, L.; Roy, C. Carbon 2000, 39, 1147.
6. Schwarz, M.-K.; Bauhofer, W.; Schulte, K. Polymer 2002, 43, 3079.
7. Busmann, H.-G.; Günther, B.; Meyer, U. Nanostruct Mater 1999, 12, 531.
8. Mamunya, Y. P.; Davydenko, V. V.; Pissis, P.; Lebedev, E. V. Eur Polym J 2002, 38, 1887.
9. Choi, M. H.; Jeon, B. H.; Chung, I. J. Polymer 2000, 41, 3243.
10. Thongruang, W.; Spontak, R. J.; Balik, C. M. Polymer 2002, 43, 2279.
11. Omastová, M.; Košina, S.; Pionteck, J.; Janke, A.; Pavlinec, J. Synth Met 1996, 81, 49.
12. Omastová, M.; Pavlinec, J.; Pionteck, J.; Simon, F.; Košina, S. Polymer 1998, 39, 6559.
13. Omastová, M.; Chodák, I.; Pionteck, J. Synth Met 1999, 102, 1251.
14. Dhawan, S. K.; Singh, N.; Rodrigues, D. Sci Technol Adv Mater 2003, 4, 105.
15. Kale, V.; Moukwa, M. J Electrostatics 1996, 38, 239.
16. Dacre, B.; Hetherington, J. I. J Electrostatics 1998, 45, 53.
17. Dudler, V.; Grob, M. C.; Mérian, D. Polym Degrad Stab 2000, 68, 373.
18. Texter, J.; Lelental, M. Langmuir 1999, 15, 654.
19. Zhou, Z.; Chu, L.; Tang, W.; Gu, L. J Electrostatics 2003, 57, 347.